NiCu-exchanged hierarchical Y and ZSM-5 zeolites for the electrochemical oxidation of glycerol

Andrea Ruggiu[a,b], Pier Parpot[c,d,*], Isabel C. Neves[c,d], Ana Paula Carvalho[e,f], Maria Giorgia Cutrufello[a,b], António Maurício Fonseca[c,d], Angela Martins[f,g], Elisabetta Rombi[a,b,*]

[a]*Department of Chemical and Geological Sciences, University of Cagliari, Complesso Universitario di Monserrato, S.S. 554, 09042 Monserrato (CA), Italy*

[b]*National Interuniversity Consortium of Materials Science and Technology (INSTM), Via Giusti 9, 50121 Florence, Italy*

[c]*CQUM, Centre of Chemistry, Chemistry Department, University of Minho, Campus de Gualtar, 4710-057 Braga, Portugal*

[d]*CEB - Centre of Biological Engineering, Universidade do Minho, Campus de Gualtar, 4710-057 Braga, Portugal*

[e]*Centro de Química Estrutural, Institute of Molecular Sciences, Universidade de Lisboa, Campo Grande 1749-016 Lisboa, Portugal*

[f]*Departamento de Química e Bioquímica, Universidade de Lisboa,Campo Grande 1749-016 Lisboa, Portugal*

[g]*Departamento de Engenharia Química, Instituto Superior de Engenharia de Lisboa, IPL, R. Conselheiro Emídio Navarro, 1, 1950-007 Lisboa, Portugal*

Abstract

Two hierarchical Y and ZSM5 zeolites were prepared with a novel surfactant-mediated desilication method. Both the conventional and hierarchical forms were used to prepare NiCu- zeolites via the ion-exchange method. All samples were characterised using different techniques. For the hierarchical

*Corresponding authors.
E-mail addresses: parpot@quimica.uminho.pt (P. Parpot), rombi@unica.it (E. Rombi).

materials, N_2 physisorption and TEM analyses confirmed the appearance of mesoporosity. Metal-containing zeolites were used for the glycerol electrochemical oxidation reaction (GEOR) in the form of modified electrodes. Cyclic voltammetry was used to investigate the surface properties of the modified electrodes and their activity toward GEOR at different pH provided by different supporting electrolyte solutions, indicating alkaline conditions as the most promising ones. The hierarchical forms showed a remarkable higher activity compared to the conventional ones, together with appreciable yields towards partially oxidated products of industrial interest. Noteworthy, a stable current higher than 10 mA was generated, which is interesting to produce H_2 by coupling GEOR and hydrogen evolution reaction.

keywords: hierarchical Y and ZSM5 zeolites; surfactant-mediated desilication; NiCu-exchanged zeolites; glycerol oxidation; electrocatalysis.

1. Introduction

In the recent years, energy production has become one of the most important challenges for the international community. The climate change and the fossil fuel shortage increase the need for alternative renewable energy sources. One promising alternative is biodiesel, the biofuels counterpart of diesel. Biodiesel is a mixture of fatty acids methyl esters obtained by trans-esterification of triglycerides in which large amounts of glycerol are also produced. Biodiesel industry is rapidly raising and is expected to grow even more in the near future. This reality has led to an overproduction of glycerol that is projected to increase in the next years. The effects of the surplus can be already observed in the drastic drop of glycerol price, both for crude and pure product [1].

In order to valorise glycerol and promote the biodiesel industry, new applications for glycerol are in development. One interesting path is the conversion into more valuable chemicals. Due to its nature of polyol, glycerol offers several possible approaches. An interesting one is the oxidation of the hydroxy functions, which could be done in mild conditions with different oxidising agents and

heterogeneous catalysts leading to the production of several interesting chemicals. Some of the most desired products are dihydroxyacetone (DHA), glyceraldehyde (GLAl), glyceric acid (GLAc), pyruvaldehyde (PAl), pyruvic acid (PAc), lactic acid (LAc), glycolic acid (GLCAc), oxalic acid (OXAc), and formic acid (FAc) [2,3].

A new and promising oxidation process is the glycerol electrochemical oxidation reaction (GEOR). Compared to the heterogeneous thermal oxidation, the main advantages are the milder condition (room temperature, atmospheric pressure), the absence of an oxidising agent and the higher control that the electrochemical process offers on the obtained products. Moreover, the GEOR is a candidate for replacing the oxygen evolution reaction (OER) in fuel cells for the production of hydrogen [4]. Green hydrogen will be fundamental for the energy transition. Hydrogen (H_2) could be used not only as an industrial chemical, but also as an energetic vector and for storing electricity produced from renewable sources. For the latter, electrochemical processes for the hydrogen evolution reaction (HER) like the water splitting reaction are particularly interesting. The main limitation of the classic water splitting reaction is the OER, which possesses a lower kinetics and requires large amount of energy [5-6]. If the OER is replaced with a lower potential reaction, such as the oxidation of an alcohol, the energy consumption could be significantly lower. Previous studies tried with methanol and ethanol, but crude glycerol from biodiesel industry could be more interesting because it is possible to use it without further treatment and to produce both H_2 and valuable chemicals by the GEOR [7-9].

The majority of the works present in the literature for GEOR focus on the use of precious metal-based catalysts. Au, Pd, and Pt in several forms (electrodes made from pure metal, alloy, or supported metal) have shown remarkable results but also have several drawbacks. Precious metals are very expensive and easily poisoned or deactivated by some of the possible products of the GEOR. To overcome this issue, they generally need the presence of other metals (noble or non-noble) and specific reaction conditions to halt the deactivation [9-12]. A possible alternative to the use of noble metals is their replacement with non-noble transition metals like Cu, Co, Fe, and Ni. Among them,

Ni is one of the most interesting since it is very cheap and well-known for its use as electrode for both oxidation and reduction electrochemical reactions of alcohols [13,14].

Electrodes prepared with Cu, Co, Fe, and Ni were previously studied for the GEOR. Oliveira *et al.* studied either Ni alone or with Co and Fe, supported on carbon, in strong alkaline conditions. They proposed that the redox activity of the superficial Ni-species is responsible for the oxidation of glycerol and that the presence of Co and Fe enhances the performances, leading to the C-C cleavage and producing a large amount of formic acid [15,16]. Zhang *et al.* prepared a series of self-standing electrodes consisting of Cu, Ni, and CuNi alloy supported on activated carbon felt (ACF) and the presence of Cu enhances the current density generated by the Ni-based electrodes. Moreover, they showed how the pH and the applied potential influenced the selectivity toward specific products, leading to the formation of either formic acid or a mixture of less oxidised C2 and C3 products [17].

Almost all the published works on the GEOR are focused on either metal alloy electrodes or carbon-supported metal catalysts. Currently, there are no published works on the use of zeolites or hierarchical zeolites. Zeolites are aluminosilicate crystalline materials with a well-ordered microporous system, characterized by large surface areas, high thermal and chemical stability, and a peculiar acidity. They are applied in several areas as cation-exchangers, adsorbents, and heterogeneous catalysts [18]. Zeolites are also used as support for metal catalysts: metal-exchanged zeolites prepared via ion exchange are very cheap, stable and show remarkable activity even with low metal loads [19]. One possible drawback of zeolites is the limited diffusion inside the micropore system, which could be detrimental for the catalytic activity of the metal-exchanged zeolites. Hierarchical zeolites represent an interesting solution because they possess a unique micro and mesoporous framework with enhanced diffusivity. They were firstly obtained as a consequence of other post-synthetic modifications, like desilication or dealumination. In the recent years several studies have shifted their attention to the intentional production of hierarchical zeolites with tuned mesoporosity, mostly because hierarchical zeolites show enhanced catalytic activity with respect to classic microporous zeolites [20-22].

In this work, the hierarchical Y and ZSM-5 zeolites were prepared with an innovative surfactant-mediated desilication method and used to prepare metal-exchanged zeolites with Cu and Ni via the ion-exchange method. By modifying the electrodes with the metal-exchanged zeolites, these modified electrodes were tested as catalysts for the GEOR and compared with standard metal exchanged Y and ZSM5 zeolites to evaluate the effect of the mesoporosity on the catalytic activity. All the modified electrodes were tested in alkaline or acidic conditions to assess the effect of the pH on the GEOR activity, the product distribution, and the generated current density. Both the hierarchical metal-exchanged zeolites showed remarkable glycerol conversion toward different products, generating a stable and intense current for several hours.

2. Experimental

2.1. Materials

Citric acid (99.5 %), glycerol (99.0 %), and nickel(II) nitrate hexahydrate (99.99 %) were supplied by Sigma-Aldrich. Cetyltrimethylammonium bromide (CTAB), nitric acid (65 %), sodium bicarbonate (> 99.7 %), sodium carbonate (> 99.5 %), sodium hydroxide (>98 %), sodium sulphate (> 99.0 %), and sulfuric acid (98 %) were purchased from Merck. Ammonia (99.99%) and nitrogen (99.99%) were supplied by SIAD and Alphagaz 1, respectively. Copper(II) nitrate hemipentahydrate (98%) was purchased from Riedel de Haen. NaY (NaY CBV-100 Si/Al = 2.8) and NH_4ZSM5 (CBV 3024E Si/Al = 15) zeolites in powder form were provided by Zeolyst International.

2.2. Preparation of hierarchical zeolites

The commercial NaY (Y_micr) and NH_4ZSM5 (ZSM5_micr) zeolites were modified through a surfactant-mediated desilication treatment, optimised from a method reported in previous works, in order to obtain the hierarchical forms [22,23].

Prior to desilication, the zeolites were submitted to different pretreatments. Y_micr was acid-washed with a 10 wt% citric acid solution to fragilize the structure, using 2 mL of solution (i.e.,

ca. 1 mmol of citric acid) for 1 g of zeolite. After around 17 h under stirring at room temperature (RT), the solid was recovered by filtration, washed, and dried at 110 °C overnight. In the case of ZSM5_micr, before desilication, the structure was fragilized in two consecutive steps: first the zeolite was dispersed in a NaOH solution (1 M, 4 mL per gram of zeolite), stirred for 1 h at 80 °C and then filtered, washed, and dried at 110 °C overnight; subsequently, the resulting powder was dispersed in a H_2SO_4 solution (0.6 M, 4 mL per gram of zeolite) for 3 h at 80 °C, under stirring and finally filtered, washed, and dried at 110 °C overnight.

The pre-treated Y and ZSM*5* zeolites were then used to prepare the hierarchical structures through the surfactant-mediated desilication process. Typically, 1 g of zeolite was added to 64 mL of a NaOH solution (0.37 M) and to 0.7 g of CTAB. After stirring for 20 min at RT and adjusting the pH to 11 with a 2 M HCl solution, the suspension (ca. 25 mL) was transferred into a 50 mL stainless steel PTFE-lined autoclave and heated at 150 °C under autogenous pressure for 6 h. The obtained solid was then filtered, washed with distilled water, and dried overnight at 110 °C.

2.3. Preparation of metal-exchanged zeolites

For the preparation of the metal-exchanged zeolites, Ni and Cu ions were inserted into the porous structure of both parent (Y_micr and ZSM5_micr) and hierarchical zeolites (Y_hier and ZSM5_hier) via an ion-exchange procedure. In a typical procedure, 1 g of the starting zeolite was suspended in 50 mL of a solution containing both metal precursor (nitrate), each at a concentration equal to 0.001 M and stirred at 300 rpm for 24 h at RT. The obtained solid was then filtered, washed with distilled water, dried at 80 °C for 12 h, and finally calcined at 350 °C for 4 h.

2.4. Preparation of the modified electrodes

In order to test the metal-exchanged zeolites as electrocatalysts for GEOR, they were used for the preparation of the zeolite-modified electrodes. A Toray carbon paper with a surface of 2 x 4 cm^2 was first glued to a platinum electrode with conductive carbon cement, and then dried for 24 h at RT.

Next, 20 mg of the metal-exchanged zeolite were mixed in a Nafion/water solution (180 μL of Nafion and 180 μL of type-1) and the suspension was homogenised in an ultrasonic bath for 20 min. Finally, the suspension was deposited on the Toray carbon paper and dried for 24 h at RT.

2.5. Zeolites characterization

Inductively coupled plasma atomic emission spectroscopy (ICP-AES) analyses were performed with a 5110 ICP-OES spectrometer (Agilent Technologies) to quantitatively determine the metal ions (Cu, Fe, and Na) content. Each sample (ca. 0.05 g) was calcined at 500 °C for 12 h, mixed with lithium tetraborate (1:15 wt/wt), placed in a platinum crucible, and then fused at 1000 °C in a furnace for 30 min. After cooling of the melt, the resultant fusion bead was dissolved in 20 mL of a HNO_3 solution (0.80 M) at 80 °C for about 30 min and finally diluted to the desired volume by type-1 water.

X-ray diffraction analyses were performed to investigate the structural properties of the catalysts on a PanAnalytical PW3050/60X'Pert PRO diffractometer with θ/θ Bragg-Brentano geometry, equipped with X'Celerator detector and using a monochromatized Cu-Kα radiation as incident beam (40 kV-30 mA). Diffractograms were obtained by continuous scanning in a 2θ range of 5 – 40 °, with a step size of 0.017 ° 2θ and a time per step of 0.68 s. The degree of crystallinity of the Y and ZSM-5 zeolites was calculated from the relative intensity of the peaks by according to the ASTM 3906-03 and ASTM D5758 methods, respectively [24,25]. Peak integration was made using Origin2021 software.

Textural analyses were carried out with an ASAP 2010 (Micromeritics) by determining the nitrogen adsorption/desorption isotherms at -196 °C. Prior to analysis, the samples (~ 70 mg) were outgassed under vacuum (7.5×10^{-5} Torr) at 300 °C for 2 h. For the evaluation of the mesopore size distribution curve was used the DFT method. The quantitative analysis of the micro and mesoporosity was made applying the α_s-method using the isotherms of a non-porous silica as reference [26].

Transmission Electronic Microscopy (TEM) was carried out with a Hitachi (Chiyoda, Japan) model H-8100 (TEM) microscope for the investigation of the morphological properties of the materials.

2.6. Modified electrodes characterization

The redox behaviour of the metal-exchanged zeolites was studied using the cyclic voltammetry technique. The voltammograms were recorded using a one-compartment with a three-electrode configuration, either with or without the glycerol in the supporting electrolyte. Two different supporting electrolytes were used to study the effect of the pH on the redox behaviour of the electrodes: pH 3, H_2SO_4 5 x 10^{-4} M with Na_2SO_4 (0.1 M); pH 10, $NaHCO_3/Na_2CO_3$ buffer (0.1 M). A surface area of 2 x 2 cm^2 Pt foil and a saturated calomel electrode (SCE) were used as the counter and the reference electrodes, respectively. The voltammograms of the working electrodes were acquired at a scan rate of 50 mV/s with a potentiostat type DT2101 (Hi-tek instruments England), coupled to a computer through an AD/DA converter. The Labview software (National Instruments) and a PCI-MIO-16E-4 I/O module were used for generating and applying the potential program as well as acquiring data such as current intensities. All the potentials were converted to reversible hydrogen electrode (RHE). Before each cyclic voltammetry analysis, the electrolytic cell was purged with Ar for 20 min.

2.7. Glycerol electrocatalytic oxidation reaction

The electrolyses of glycerol were carried out under atmospheric pressure and RT in a membrane separated two-compartment electrochemical cell (250 mL for each compartment) with a three-electrode configuration, using a Pt foil as counter electrode and a saturated calomel electrode as reference. In each experiment, the working electrode cell was filled with 250 mL of the solution of glycerol (0.01 M) and supporting electrolyte, while the counter electrode cell was filled with 250 mL of the same supporting electrolyte solution. Then, a constant potential was applied to the working

electrode during electrolyses, stirring both the solutions. After 30 minutes and subsequently after each hour of reaction, 0.5 mL of the reaction mixture were taken and analysed by a high-performance liquid chromatograph (HPLC), equipped with a Jasco PU-980 HPLC pump, a Jasco UV-975 detector, and a Shimadzu RID-6A refractive index detector (RID). The analysis was performed at RT using an Aminex HPX-87H column from BIORAD, an injection volume of 20 μL, a flow rate of 0.5 mL min^{-1}, and the UV detector at a wavelength of 210 nm. Solutions of known concentrations of the different standards were prepared and used to determine the retention times and calibration curves. The amount of glycerol (GLY), dihydroxyacetone (DHA), glyceraldehyde (GLAl), glyceric acid (GLAc), glycolic acid (GLCAc), tartronic acid (TAc), oxalic acid (OXAc), and formic acid (FAc) was assessed. The percentage conversion of GLY was calculated according to Eq. 1; the percentage selectivity to each product was calculated according to Eq. 2:

$$X_{\mathrm{GLY}} = \frac{(n_{\mathrm{GLY,initial}} - n_{\mathrm{GLY,final}})}{n_{\mathrm{GLY,initial}}} \times 100 \quad (1)$$

$$S_{\mathrm{Product}} = \frac{(n_{\mathrm{Product}})}{(n_{\mathrm{GLY,initial}} - n_{\mathrm{GLY,final}})} \times 100 \quad (2)$$

3. Results and discussion

3.1. Zeolites and metal-exchanged zeolites characterization

The XRD patterns of the starting and modified Y and ZSM5 zeolites are reported in Fig. 1a and 2a, respectively. Both the Y zeolites show the typical structure of the faujasite-type zeolites, whereas for the ZSM5, the observed pattern is the one typical of the MFI zeolites. To quantify the loss of crystallinity due to the modification treatments, the degree of crystallinity (C_{XRD}) was calculated from the relative intensity of selected peaks, using the starting zeolites as the reference [24,25]. The results, reported in Tab. 1, show a marked decrease in the C_{XRD} for the Y_hier zeolite, whereas, for the ZSM5_hier sample, the crystallinity loss is less significant. This points out that the desilication treatment promotes a greater modification of the crystalline structure for the former zeolite than in the latter one.

Tab. 1. Structural and textural properties of the zeolites

Sample	C_{XRD}[a] (%)	V_{ultra}[b] ($cm^3\ g^{-1}$)	V_{super}[b] ($cm^3\ g^{-1}$)	V_{meso}[b] ($cm^3\ g^{-1}$)
Y_micr	100	0.33	0.01	0.01
Y_hier	37	0.16	0.08	0.07
ZSM-5_micr	100	0.13	0.03	0.08
ZSM-5_hier	91	0.11	0.02	0.22

[a]assessed from XRD patterns
[b]assessed by the application of the α_s-method to the N_2 physisorption isotherms

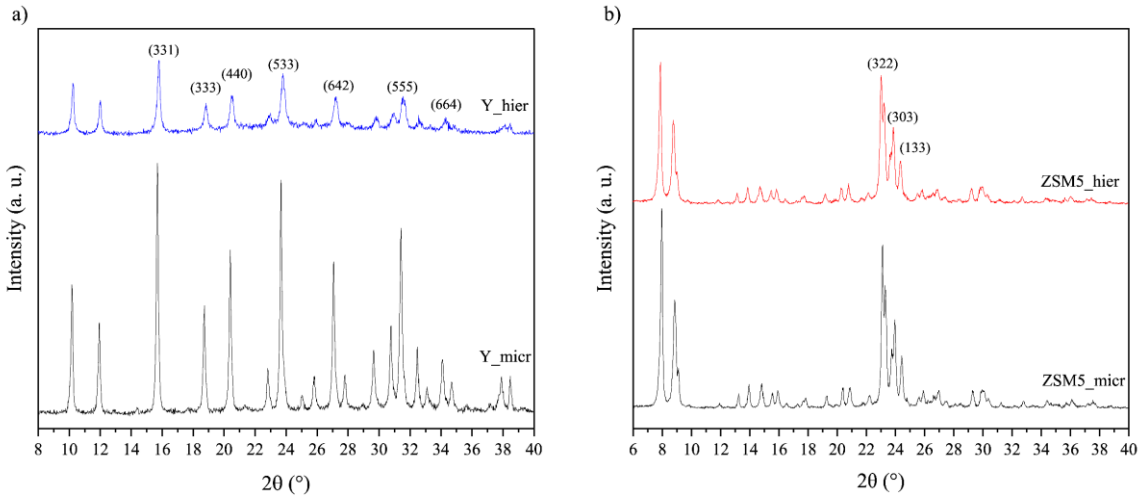

Fig. 1. X-ray diffraction patterns of a) Y and b) ZSM5 zeolite samples.

The N_2 adsorption-desorption isotherms at –196 °C of the Y and ZSM5 zeolites are reported in Fig. 2a and 2c respectively, whereas the textural properties are summarized in Tab. 1. As expected, both the Y_micr and ZSM5_micr zeolites show type I isotherms, typical for microporous materials. The upward deviation observed in the high relative pressure region, especially in the ZSM5_micr isotherm, can be ascribed to the aggregation of small crystals, resulting in intercrystalline porosity. A pronounced upward deviation at high relative pressures, with a typical H4 hysteresis loop, is observed for the hierarchical samples. In both cases the isotherms can be classified as type I + IV, indicating the simultaneous existence of micro and mesopore systems even though the isotherm configurations are quite different. For the Y_hier zeolite, the most important feature is the appearance,

in the adsorption branch of the isotherm, of an accentuated step between p/p^0 0.3 and 0.5, which suggests the development of wider micropores and/or narrow mesopores, according to what reported in the literature [22,23].

The micropore volume (V_{micro}) was assessed by the α_s-method, which also allows distinguishing between the volume of ultramicropores (V_{ultra}, $\varphi < 0.7$ nm) and supermicropores (V_{super}, 0.7 nm $< \varphi <$ 2 nm). The mesopore volume (V_{meso}) was determined by the difference between the total pore volume (V_{total}) at p/p^0 ca. 0.95, and V_{micro}. Compared to the parent Y_micr, the values obtained for Y_hier (Tab. 1) reveal that the desilication treatment led to the development of supermicropores and mesopores (increased V_{super} and V_{meso} values) at the expense of the original ultramicropores (decrease in V_{ultra}). For the ZSM5_hier sample, the treatment did not induce any modification in the micropore network, whereas an important formation of mesopores is observed (V_{meso} remarkably increases), suggesting that mesoporosity is probably interparticle.

In Fig. 2b and 2d, the pore size distribution curves obtained by DFT method are reported for the Y and ZSM5 zeolites, respectively. Compared to Y_micr, which, as expected, does not exhibit any mesoporosity, the Y_hier sample shows a monomodal mesopore distribution with a significant contribution centred at 4 nm. This suggests that CTAB has efficiently produced intraparticle mesoporosity [23]. Noteworthy, the ZSM5_micr zeolite, in which only intraparticle micropores are expected, shows a bimodal distribution with contributions around 2-3 nm and between 10 and 40 nm, the latter being mainly ascribable to inter-particles mesoporosity, in line with what already reported in the literature [23].

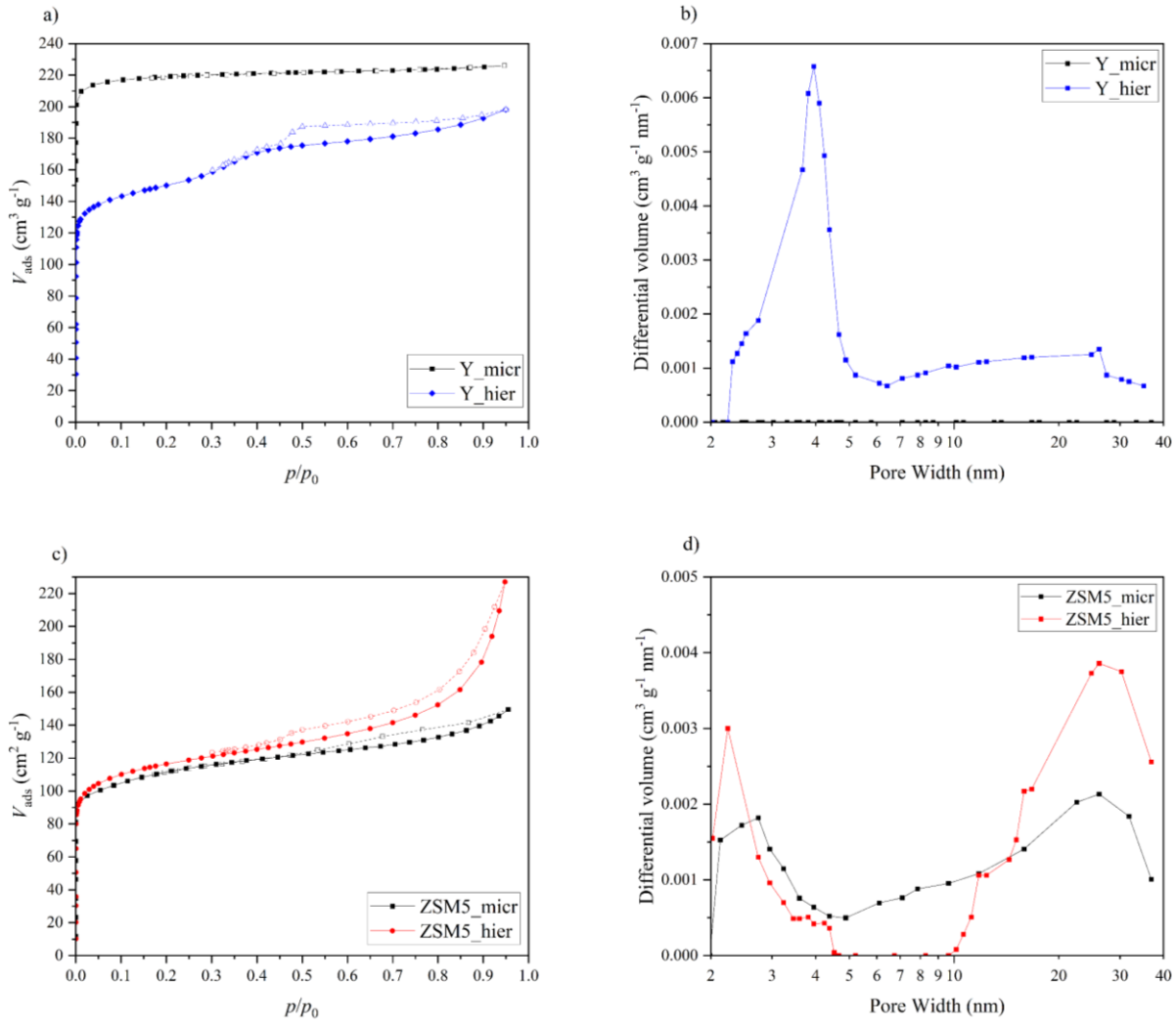

Fig. 2. a) and c) N_2 physisorption isotherms of the Y and ZSM-5 zeolites (adsorption: solid line, desorption: dashed line), respectively; and b) and d) pore size distribution of the Y and ZSM-5 zeolites obtained with the DFT method, respectively.

The TEM micrographs of the Y_micr, Y_hier, and ZSM5_hier samples are reported in Fig. 3 and Fig. S1. Compared to the smooth surface of the starting Y_micr zeolite (Fig. 3a), the external surface of the Y_hier particles (Fig. 3b) turns up rougher and damaged, as a consequence of the desilication process. Also the hierarchical ZSM5 sample (Fig. 3c) appears damaged, as expected considering the harsh treatments involved. Furthermore, the formation of aggregates of small particles can be observed, confirming the hypothesis of an interparticles mesoporosity, in agreement with the N_2 physisorption results. It is worthy of note that several lighter spots are observable in the

micrographs of both the hierarchical samples, which, according to the literature can be attributed to the structural modification induced by the surfactant-mediated desilication [23].

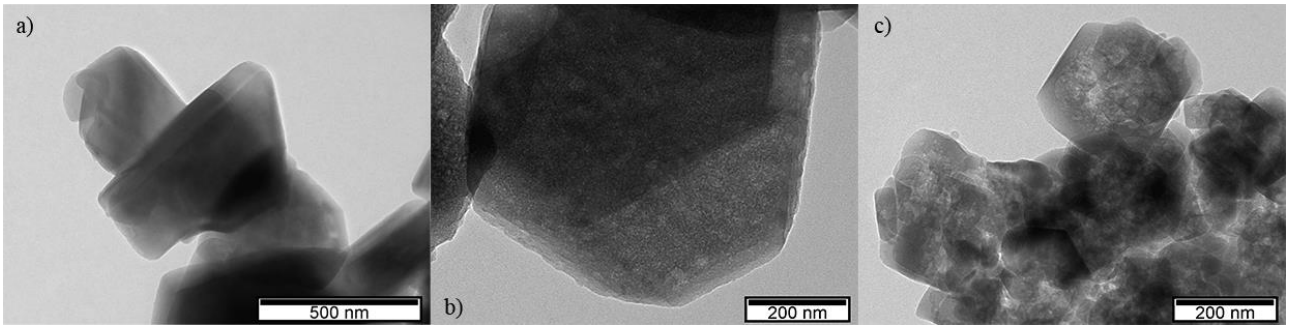

Fig. 3. TEM micrographs of the zeolites series: a) Y_micr; b) Y_hier and c) ZSM5_hier.

The chemical composition and the textural properties of the metal-exchanged zeolites are reported in Tab. 2. The elemental analysis shows that the ion exchange process was effective for the introduction of the Ni and Cu metal ions in the Y zeolites, the metals content being the same in NiCuY_micr and NiCuY_hier. On the contrary, in the case of ZSM5 samples, the process is efficient only for loading Cu, since only a very small amount of Ni is present in the final metal-exchanged zeolites. However, the amount of both metal ions is higher in NiCuZSM5_hier than in NiCuZSM5_micr. This is likely due to the presence of large mesopores in the hierarchical sample, which facilitate the diffusion of the metal precursor within its porous structure.

The N_2 physisorption results on the metal-exchanged Y and ZSM-5 zeolites are reported in Fig. S2 and the textural parameters summarized in Tab. 2. Both the isotherms and the pore size distribution curves of the metal-exchanged zeolites are very similar to those of the parent ones (cnf. Fig. 2), indicating that the textural properties are only slightly affected by the insertion of the metal ions.

The XRD data of the metal-exchanged zeolites are reported in Figs. S3a and S3b for the Y and ZSM5 series, respectively. All the samples are crystalline, with the typical pattern of the faujasite structure for the Y samples and that of the MFI structure for the ZSM5 ones. For both the standard and the hierarchical zeolites, the degree of crystallinity does not change with the ion exchange

process, further confirming that the introduction of the metal ions does not modify the zeolite framework.

Tab. 2. Chemical composition and structural and textural properties of zeolites and metal-exchanged

Sample	Metal content [a] (wt%)			V_{ultra} [b] (cm^3/g)	V_{super} [b] (cm^3/g)	V_{meso} [b] (cm^3/g)
	Na	Cu	Ni			
Y_micr	8.82	/	/	0.33	0.01	0.01
Y_hier	5.75	/	/	0.16	0.08	0.07
NiCuY_micr	8.23	0.45	0.38	0.30	0.03	0.01
NiCuY_hier	5.76	0.46	0.37	0.14	0.07	0.07
ZSM5_micr	0.80	/	/	0.13	0.03	0.08
ZSM5_hier	0.95	/	/	0.11	0.02	0.22
NiCuZSM5_micr	0.00	0.35	0.10	0.11	0.03	0.08
NiCuZSM5_hier	0.89	0.41	0.18	0.12	0.01	0.25

[a]assessed by ICP-OES analysis
[b]assessed by the application of the αs-method to the N_2 physisorption isotherms

3.2 Cyclic voltammetry

The cyclic voltammograms of the NiCuY-modified electrodes, prepared with parent (NiCuY_micr) or hierarchical (NiCuY_hier) zeolites are displayed in Fig. 4. The voltammograms recorded at pH 3 (5 mM H_2SO_4 + 0.1 M Na_2SO_4), without glycerol (Figs. 4a and 4c, black line), show a redox process attributed to the Cu(I)/Cu(0) couple with anodic and cathodic peaks at 0.47 and 0.23 V vs. RHE, respectively. Besides this redox process, an additional redox couple with peak potentials at 0.80/0.78 V vs. RHE can be noticed on the voltammogram of NiCuY_hier (Fig. 4c), whose current intensities, ascribed to the Cu(II)/Cu(I) couple, are much lower than those found for the Cu(I)/Cu(0) one. The presence of the Cu(II)/Cu(I) redox couple in the NiCuY_micr zeolite cannot

be also excluded, as it may be hidden by the intense peak generated by the Cu(I)/Cu(0) couple. The separation of these two redox processes and the higher current intensities indicates an increased accessibility of copper in the hierarchical zeolite, due to the enhanced diffusivity within its wider micropores and mesopores. No clear evidence of the redox activity of Ni can be noticed, due to the lack of nickel oxyhydroxide (NiOOH) formation in acidic medium. The additional cathodic peak around -0.25 V vs. RHE observed for NiCuY_hier could be attributed to the reduction of oxygen, formed during the anodic scan, and trapped in the zeolite framework [27]. In the presence of glycerol (Fig. 4a, red line), an increase in the current intensities was noticed for NiCuY_micr, starting from 0.45 V vs. RHE, which can be ascribed to the formation of Cu(I) species. These results suggest that the oxidation of glycerol, at lower potentials, needs the presence of Cu_2O species to enable the charge transfer (Eq. 3):

$$\text{Organic compound} + Cu_2O \rightarrow 2\ Cu(0) + \text{Oxidation product} \quad (3)$$

The current intensities of glycerol oxidation obtained with NiCuY_hier (Figure 4c, red line) in the stability region of water are lower than those obtained with the parent sample. This indicates that surface deactivation due to the irreversible adsorption of the initial substrate and/or reaction products is more significant in this case.

In the absence of glycerol, unlike what observed in acidic medium, the redox process related to the Cu(II)/Cu(I) couple can be observed in alkaline medium (pH 10, $NaHCO_3/Na_2CO_3$ (0.1 M)) for both the parent and hierarchical NiCuY zeolites (Figs. 4b and 4d). However, the peaks related to this redox process are not clearly apparent, due to an easier OH adsorption on copper in this medium, which keeps the surface partially oxidized by adsorbed oxygenated species in a wider range of potentials. For the hierarchical zeolite, the distance between the anodic and cathodic peaks, at 0.8 and 0.6 V vs. RHE, respectively, is lower than that found for the parent one, whose peaks are observed at 1.0 and 0.6 V vs. RHE during the positive and negative variation of potential, respectively. The shorter distance between the anodic and cathodic peaks observed for NiCuY_hier highlights an

enhanced reversibility of the redox process, and therefore a higher reaction rate, on the hierarchical zeolite compared to parent one.

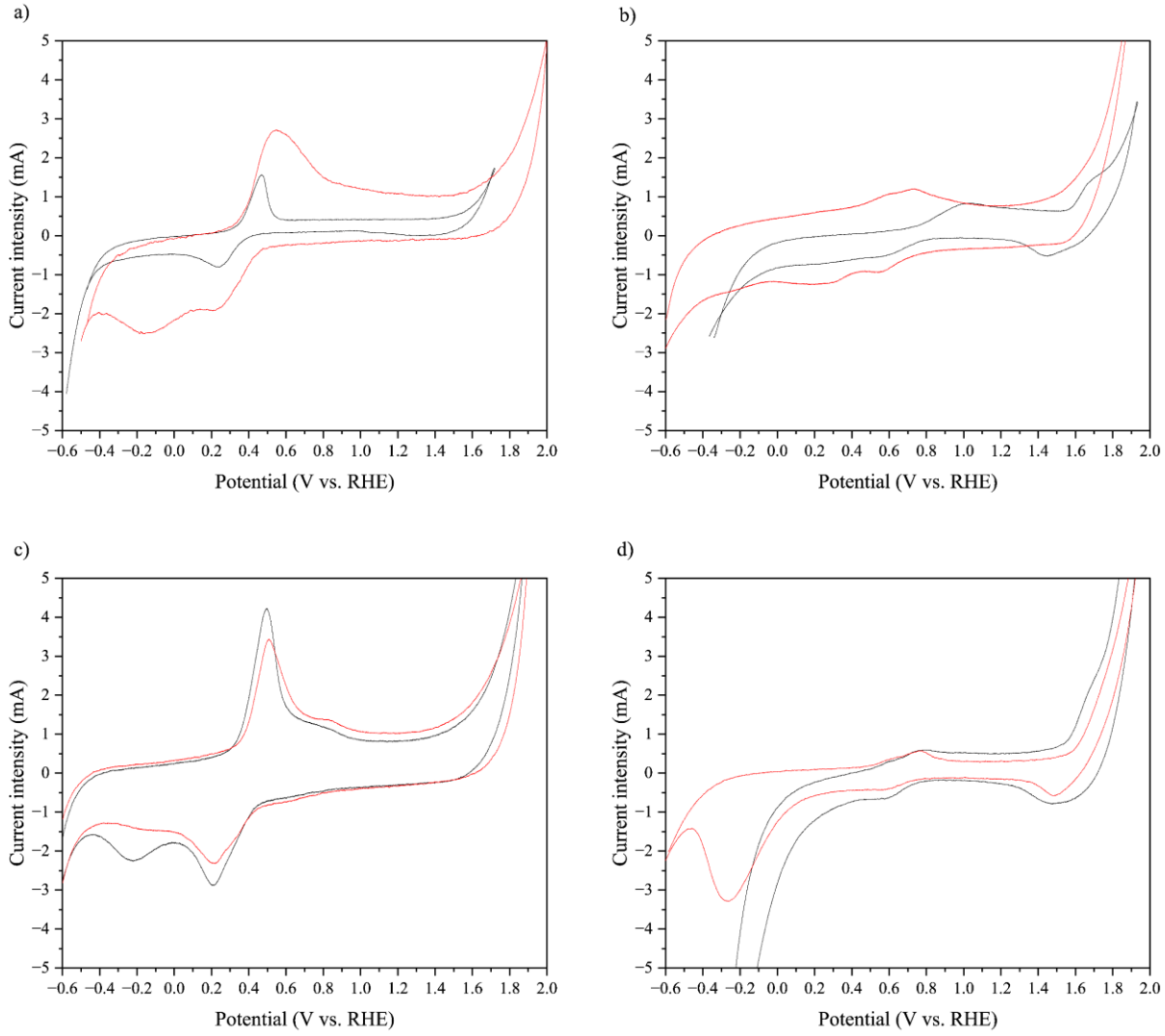

Fig. 4. Cyclic voltammograms of the modified electrodes based on NiCuY series, registered at 50 mV/s scan ratio in absence (black line) and presence (red line) of glycerol 0.01 M, in different supporting electrolyte solutions: a) NiCuY_micr and c) NiCuY_hier, in H_2SO_4 (5 mM) and Na_2SO_4 (0.1 M); b) NiCuY_micr and d) NiCuY_hier in Na_2CO_3/$NaHCO_3$ (0.1 M).

The second redox process between 1.5 and 1.8 V vs. RHE occurs in the nickel oxyhydroxide (NiOOH) region, just before the oxygen production, and can be attributed to the contribution of nickel, according to Eq. 4 [28]:

$$Ni(OH)_2 + HO^- \rightarrow NiOOH + H_2O + e^- \quad (4)$$

The redox peaks ascribed to the Ni(III)/Ni(II) couple are more pronounced in the voltammogram of the parent zeolite compared to the hierarchical one, which shows the superimposition of narrow peaks corresponding to the metal oxide (NiO_x) formation and the oxygen evolution, respectively. This fact shows that the oxidation of $Ni(OH)_2$ toward the metal oxide rather than NiOOH formation was privileged in this last case. The mechanism involved is a hydroxide-mediated deprotonation in which a negatively charged surface oxide (O_{ads}^-) is formed according to Eq. 5, and the subsequent O_2 formation occurs through the decomposition of this oxide [29].

$$Ni(OH)_2 + 2\ HO^- \rightarrow NiOO^{2-} + 2\ H_2O \quad (5)$$

This behaviour in the hierarchical zeolite could be related to a probably higher local concentration of OH^- ions.

In the presence of glycerol, the voltammograms of both the parent and hierarchical NiCuY zeolites modified electrodes (red lines in Figs. 4b and 4d, respectively) show significant differences compared to those obtained in the supporting electrolyte medium alone. The hydrogen evolution on the electrode surface is shifted to more cathodic potentials, indicating a significant coverage of the active sites by the organic compounds, which makes the adsorption and further reduction of H^+ ions more difficult. The significant increase in current intensities during the anodic scan, starting from 1.4 V vs. RHE, for the parent NiCuY_micr modified electrode (Fig. 4b, red line) confirms the oxidation of glycerol by the NiOOH species, according to the redox cycle in Fig. 5. In this case the Ni(III)/Ni(II) couple can act as the mediator to oxidize the organic species [28].

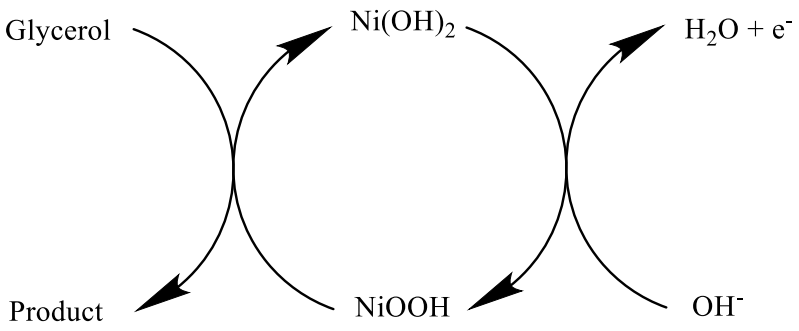

Fig. 5. Catalytic cycle of the glycerol electrooxidation process on the Ni-containing modified electrodes based on the metal-exchanged zeolites [28].

The overlay of the resulting current intensities with those produced by further oxygen evolution makes it difficult to obtain a well-defined oxidation peak. Unlike what noticed for the NiCUY_micr modified electrode, no significant current intensities are observed in the voltammogram of the NiCuY_hier one (Fig. 4d, red line) in the NiOOH region, suggesting that in this case the oxidation of glycerol might take place on non-redox trivalent nickel species. In this mechanism the nucleophilic hydroxyl groups of glycerol interact with the electrophilic NiOOH species *via* a nucleophilic attack, followed by a direct non-redox electron extraction from glycerol, without an intermediate reduction of NiOOH to $Ni(OH)_2$ [30].

The contribution of metal oxide sites in glycerol oxidation decreases their availability for oxygen production and shifts the potential related to this process to more anodic values. The earlier hydrogen evolution on the NiCuY_hier modified electrode (Fig. 4d, black line), at lower cathodic potentials, indicates its higher affinity for hydrogen adsorption compared to the NiCuY_micr one (Fig. 4b, black line). This fact could explain the preference for an oxidation on copper oxide at higher potentials, rather than at lower potentials on copper species in lower oxidation states. In this case, the reduction of the copper species with lower oxidation state, like Cu(I) to metallic Cu by the adsorbed hydrogen can be expected (Eq. 6), decreasing the availability of the former for the oxidation of organic compounds.

$$2H_{(ad)} + Cu_2O \rightarrow 2\,Cu(0) + H_2O \qquad (6)$$

The cathodic peaks observed during the negative variation of potential might be related to the reduction of the oxidation products formed during the anodic scan. The difference observed in the reduction potentials also suggests that different products are formed on the parent and hierarchical zeolites.

The modified electrodes based on both the conventional and hierarchical NiCuY zeolites appear to be able of oxidizing glycerol to some extent, making them worthy of further investigation in electrocatalytic oxidation tests.

The cyclic voltammograms of either the modified electrodes with either the parent NiCuZSM5_micr or the hierarchical NiCuZSM5_hier zeolites are reported in Fig. 6. For both electrodes, the voltammograms recorded in acid medium without glycerol (black lines in Fig. 6a and 6c) show peaks ascribable to the Cu(I)/Cu(0) and Cu(II)/Cu(I) redox couples at 0.40/0.35 and 0.85/0.80 V vs. RHE, respectively. Such redox processes are more discernible and better separated with these modified electrodes, compared to the NiCuY-based ones. In the presence of glycerol (red lines in Figs. 6a and 6c), these peaks are less pronounced and mostly overlapping with those of moderate current intensity generated by glycerol oxidation, suggesting an oxidation mechanism mediated by Cu(I) species analogue to the one described for the NiCuY-modified electrodes (Eq. 3).

In alkaline medium (Fig. 6b and 6d), an inhibition of charge transfer reactions up to 0.8 V vs. RHE can be noticed, due to the glycerol adsorption on the surface. Nevertheless, a glycerol oxidation process with moderate current intensities is observable between 0.80 and 1.20 V vs. RHE on the NiCuZSM5_micr-modified electrode (Fig. 6b, red line). An oxidation mechanism mediated by Cu(II) species can be suggested in this case (Eq. 7):

$$GLY + Cu(II) \rightarrow Cu(I) + \text{oxidation products} \quad (7)$$

This process is not observed using the hierarchical zeolite (Fig. 6d), since in this case the oxidation of glycerol occurs at higher anodic potentials, as described earlier for the NiCuY_hier-modified electrode.

In the absence of glycerol, the voltammograms of the conventional and hierarchical NiCuZSM5 modified electrodes (black lines in Fig. 6) do not exhibit any redox processes in the NiOOH region. This finding may be related to the small amount of nickel (Tab. 2) and to its availability for the electrochemical redox process. In fact, as previously reported in the literature for Ni-ZSM5 catalysts, for metal contents up to 0.4 wt% nickel is located inside the ZSM5 pores only as the compensation cation [31]. Nonetheless, an oxidation mechanism mediated by non-redox trivalent nickel species through a nucleophilic attack on Ni(III) active species by hydroxyl groups of glycerol cannot be ruled out.

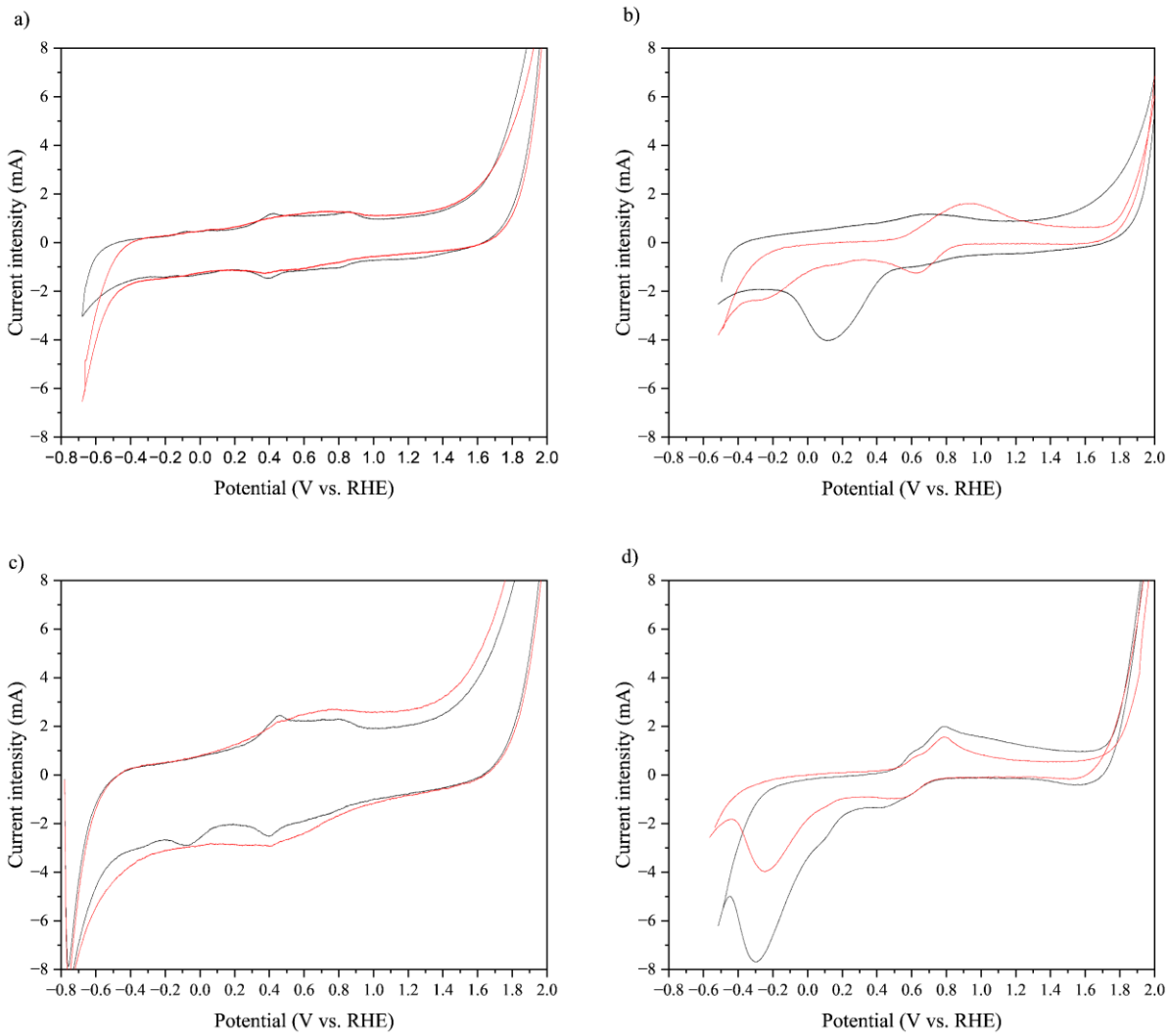

Fig. 6 - Cyclic voltammograms of the modified electrodes based on NiCuZSM-5 series, registered at 50 mV/s scan ratio in absence (black line) and presence (red line) of glycerol (0.01 M), in different

supporting electrolyte solutions: a) NiCuZSM5_micr and c) NiCuZSM-5_hier in H_2SO_4 (5 mM) and Na_2SO_4 (0.1 M); b) NiCuZSM5_micr and d) NiCuZSM5_hier in Na_2CO_3/$NaHCO_3$ (0.1 M).

3.3 Glycerol electrochemical oxidation reaction tests

All the prepared modified electrodes based on zeolites were studied in the electrocatalytic oxidation of glycerol. The electrolysis of GLY was performed in acid or alkaline conditions by either applying a fixed potential or using a program of variation of the potential, which includes different potential pulses.

Under acidic conditions, a constant potential of 0.5 V vs. RHE, corresponding to the oxidation of Cu species, was first applied to the electrodes modified with both the parent and hierarchical NiCuY zeolites, observing an initial current intensity of ca. 10 mA, which however dropped to less than 1 mA after a few minutes. This rapid deactivation of the modified electrode, probably caused by the irreversible adsorption of oxidation products like CO, inhibited the long run electrolysis. The same behaviour is observed when the potential is varied using a program consisting of three pulses: first a 1 s activation pulse at -0.5 V vs. RHE, then a 20 s pulse at 0.5 V vs. RHE, and finally a 1 s cleaning pulse at 1.8 V vs. RHE.

In order to decrease the deactivation rate, the electrolysis was performed at a more positive potential value, i.e. 1.7 V vs. RHE, just before oxygen evolution. For both the NiCuY-based electrodes, current intensities in the range 5-7 mA were observed, although accompanied by oxygen production. However, after few hours of test the current intensities dropped to less than 1 mA, without glycerol conversion. Similar results were obtained using the NiCuZSM5-modified electrodes, showing that with both the parent and hierarchical zeolites, at low potentials, the deactivation of the electrode surface does not allow the conversion of glycerol, while at more anodic potentials the only redox reaction is the oxygen production.

Taking into account the previous results, further electrolyses were carried out in alkaline medium. In this case, for both the Y and ZSM-5 zeolites, a rapid deactivation of the modified

electrodes was still observed with a constant applied potential of 0.7 V vs. RHE, where copper is in its oxidized form (Cu(II)). The use of a potential variation program, which consisted of a 1 s pulse at -0.4 V vs. RHE for activation, a 20 s pulse at 0.7 V vs. RHE for oxidation, and a 1 s pulse at 2.1 V vs. RHE to clean the electrode, allowed the generation of stable current intensities of approximately 4-5 mA. Nevertheless, GLY conversion remained very low (< 5 mol%).

Higher anodic potentials, in the Ni oxides region, allowed maintaining satisfactory current intensities, using both the parent zeolites (NiCuY_micr and NiCuZSM5_hier) modified electrodes. A wide range of potential values (from 1.5 V to 2 V vs. RHE) was investigated with the aim of identifying the lowest potential which provides a stable and relatively high current intensities, while avoiding oxygen evolution. The optimal values of 1.85 and 2.0 V vs. RHE, corresponding to the current intensities of 3 and 7 mA were found for NiCuY_micr and NiCuZSM5_micr, respectively. The substitution of parent zeolites with hierarchical ones significantly enhances the performance in the electrochemical oxidation of glycerol. The electrolysis using the NiCuY_hier-modified electrode at 1.85 V vs. RHE provided an initial current intensity of approximately 3 mA, which progressively increased up to 18 mA after 5 h, and then stayed constant until the 15^{th} hour of test, before a gradual decrease down to 8.2 mA at the end of the electrolysis, after 21 h. No oxygen formation was noticed during the process. Concerning the NiCuZSM-5_hier-modified electrode, tested at 2.0 V vs. RHE, a current intensity of 11.5 mA was initially observed. This value increased up to 14.5 mA during the first hour of electrolysis, was constant until the 16^{th} hour, and then decreased slowly down to 11.5 mA at the end of the electrolysis (21 h), without any oxygen evolution on the electrode surface. The different electrochemical behaviour observed between the NiCuY and the NiCuZSM5 modified electrodes, with both the parent and the hierarchical zeolites, can be explained considering the effect of the different Al amount on the stability of the Ni species present on the electrodes.

In the literature [27], it is reported that in alkaline medium the β-$Ni(OH)_2$ phase is more stable than the α-$Ni(OH)_2$ phase, but the presence of Al stabilises the α-$Ni(OH)_2$ phase. The potential for the α-$Ni(OH)_2$/γ-NiOOH oxidation is ca. 20-40 mV lower compared the β-$Ni(OH)_2$/β-NiOOH

oxidation. Since the Y zeolite has ca. 5 times the amount of Al than the ZSM5 zeolite, it is plausible that significantly more α-$Ni(OH)_2$ species are present, lowering the optimal potential for the electrochemical oxidation.

The electrocatalytic results are summarized in Fig. 7 in terms of glycerol conversion and products yield; the same results in terms of products selectivity are reported in Tab. S1 and S2. Comparing the performances of the two modified electrodes based on the parent zeolites, it is evident that the NiCuY_micr (Fig. 7a) is less active, showing a low glycerol conversion even after 6 h, probably due to a significant surface deactivation. The NiCuZSM5_micr-modified electrode (Fig. 7b) shows better results, especially taking into account the higher current intensity that remains stable up to 6 h. Glycerol was oxidized with moderate reaction rates, reaching 12 % of conversion after 6 h of electrolysis. GLAl is the main product for the first 3 h, GLCAc and FAc being also formed through its further oxidation. Small traces of dicarboxylic acids (TAc and OXAc) were also detected; however, in the last 2 h, CO_2 production became the main oxidation process. Noteworthy, the presence of DHA was observed only in the last hour of reaction, suggesting that its concentration was previously below the HPLC detection limit during the initial stage of the electrolysis.

The results obtained with the hierarchical zeolites are more interesting and promising. Since the beginning of electrolysis, the NiCuY_hier electrocatalyst (Fig. 7c) was more active than its parent counterpart, providing 32 % of GLY conversion after 6 h, against the 6 % obtained with NiCuY_micr. Despite the observation of a gradual decrease in current intensity from 18 mA to ca. 8 mA, the hierarchical zeolite was still active after 21 h, reaching a glycerol conversion of 52 %. The GLAl yield increased with glycerol conversion up to 19 %, being by far the main product at 21 h (GLAl selectivity = 36 mol%, Tab. S1). Contrarily to what observed with NiCuY, a small amount of DHA, whose yield stabilises around 1-2 %, was detected since the beginning. Besides GLY, mostly GLAl and DHA were oxidized to some extent. The yields toward GLCAc, FAc, dicarboxylic acids, and CO_2 increased during the first 6 h, with the latter being the main product, which suggests that the

formation of GLAl by the direct oxidation of glycerol was slower than its further oxidation within this period.

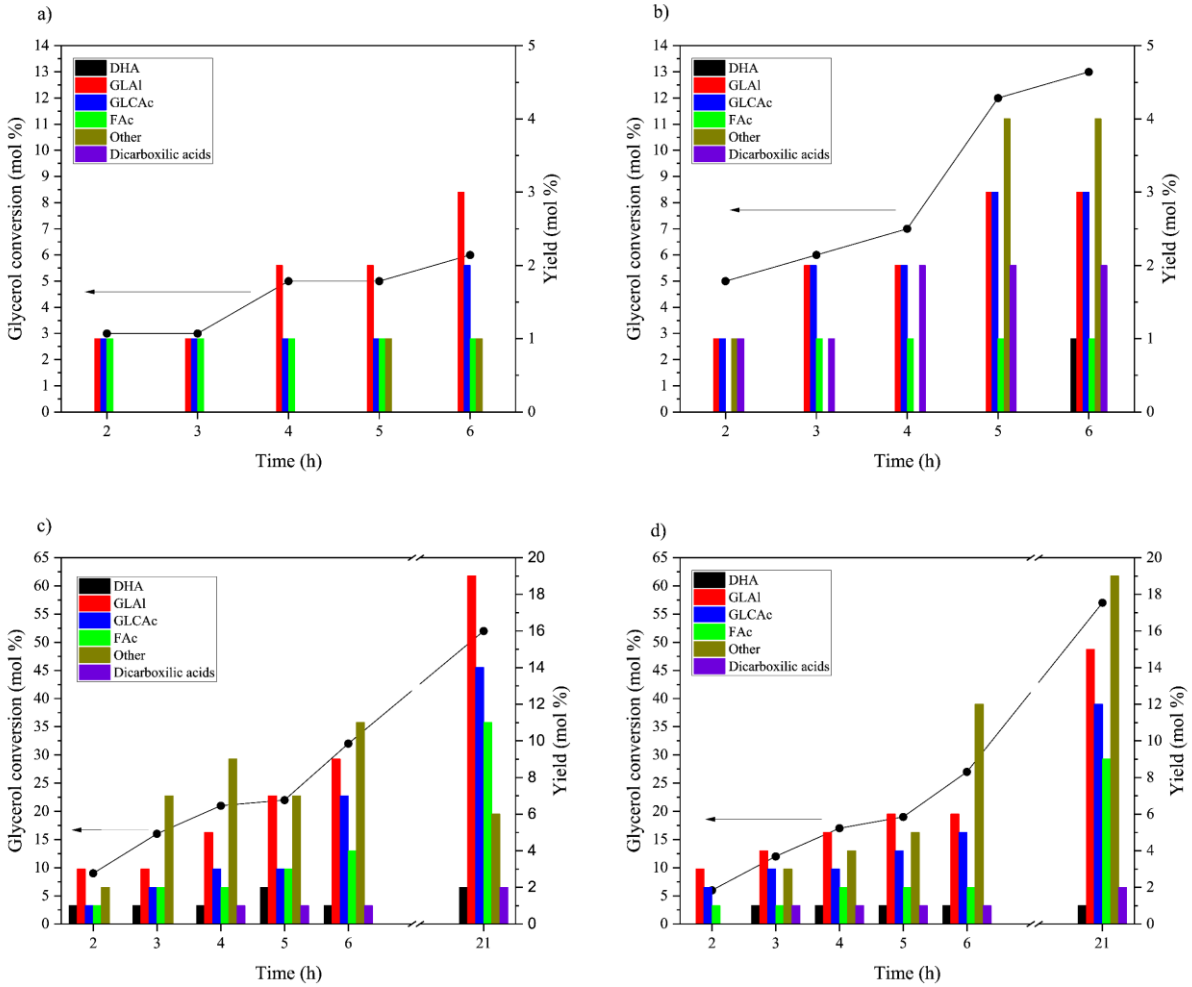

Fig. 7. Glycerol conversion (dot and line) and product yields (columns) for the GLY oxidation reaction: a) NiCuY_micr, b) NiCuZSM5_micr, c) NiCuY_hier, d) NiCuZSM5_hier modified electrodes.

The results obtained with the NiCuZSM5_hier-modified electrode are similar to the previous electrolysis(Fig. 7d). In this case, compared to the parent NiCuZSM5_micr, a two-fold increase is noticed for glycerol conversion at 6 h. The modified electrode was still active after 21 h of electrolysis despite the decrease in current intensity, which however remained stable at around 10 mA starting from the 16th hour. Noteworthy, this NiCuZSM-5_hier-modified electrode allowed achieving the

highest glycerol conversion. The products distribution (Tab. S2) is almost as the one obtained with the hierarchical NiCuY_hier zeolite, the main difference being that CO_2 is the most abundant product at the end of the test. However, GLAl is still present in high amounts, with a final yield of 15%.

Comparing the overall results obtained using the modified electrodes based on the parent and hierarchical NiCu-zeolites, it can be concluded that the hierarchical ones grant a higher electrochemical activity, promoting different oxidation mechanisms and providing a final mixture of products of increased commercial interest. The appreciable yield value of GLAl, a partially oxidised product, suggests that the hierarchical zeolites can promote glycerol oxidation over the further oxidation of the primary products. This could be reasonably explained by the enhanced diffusivity attributed to the hierarchical samples, thanks to the presence of super micropores and narrow mesopores (Table 1). Indeed, although the glycerol molecule is small enough to diffuse within the micropores of parent NiCuY_micr and NiCuZSM5_micr zeolites, its diffusion rate would be significantly lower than that within the wider micropores and mesopores of their hierarchical form. Moreover, many of the C3 products, which are even bulkier than glycerol, may hardly counter-diffuse into the bulk solution from the micropores where they are formed, thus remaining in the proximity of the active sites, where they can be further oxidised. The difficulty of counter-diffusion through the micropores also facilitates their filling, preventing the access of further glycerol to the active sites. Therefore, a greater quantity of glycerol will be able to access the active sites, while the products formed, once desorbed, can counter-diffuse more easily, limiting the possibility of being further oxidized.

4. Conclusions

The electrochemical oxidation of glycerol in mild conditions was successfully performed using hierarchical Y and ZSM5 zeolites prepared by an innovative surfactant-mediated desilication method. For the Y zeolite the treatment with CTAB promoted the formation of narrow intra-particles mesopores (approx. 4 nm), whereas in the case of ZSM5 the formation of large inter-particles

mesopores (10-40 nm) was observed. With both the parent and hierarchical Y and ZSM5, metal-exchanged zeolites containing Cu and Ni were prepared via the ion-exchange method and were used to prepare modified electrodes. Cyclic voltammetry studies were performed with the modified electrodes based on the metal-exchanged zeolites at different pH and in different supporting electrolyte medium. The results showed that alkaline conditions are the most promising for the GLY electrooxidation and indicated different mechanisms, which involve different redox couples depending on the metal-exchanged zeolite used. In particular, with the NiCuY-modified electrodes, the NiOOH and the non-redox trivalent Ni species can be considered as the active phases for NiCuY_micr and NiCu_hier, respectively. Whereas the Cu(I)/Cu(0) couple appeared to be mainly responsible for the oxidation process in the case of both the parent and hierarchical NiCuZSM5-modified electrodes. The electrolyses of GLY, performed both in acid and alkaline media by applying fixed or programmed potentials, demonstrated that alkaline conditions and high potential are necessary to allow appreciable GLY conversions. For both the NiCuY- and NiCuZSM5-based electrocatalysts, the hierarchical forms showed higher activity compared to the parent ones. After 6 h, the hierarchical NiCuY_hier provided fivefold increase in GLY conversion compared with the parent metal-exchanged zeolite (32 mol% *vs.* 6 mol%), whereas a two-fold increase was observed for the hierarchical NiCuZSM5_hier (13 mol%) compared to NiCuZSM5_micr (27 mol%). By comparing the hierarchical NiCuY_hier and NiCuZSM5_hier electrocatalysts, it was found that, at comparable GLY conversions, the former shows the most interesting results in terms of total yield towards the partial oxidation products (GLAl, DHA, GLCAc, and FAc), accounting for 46 mol%. Noteworthy, the hierarchical metal-exchanged zeolites turned out to be active in the long-term electrolysis (21 h), generating stable current intensities higher than 10 mA. This finding is worthy of further investigation considering that the generation of a stable and high-intensity current for a long time is particularly interesting to produce H_2 through the coupling of the GEOR with the hydrogen evolution reaction.

CRediT authorship contribution statement

Andrea Ruggiu: Conceptualization, Investigation, Formal analysis, Validation, Writing-Original draft, Visualization. **Pier Parpot:** Methodology, Validation, Supervision, Writing - Review & Editing. **Isabel C. Neves:** Resources, Funding acquisition, Writing - Review & Editing. **Ana Paula Carvalho:** Methodology, Supervision, Resources, Funding acquisition, Writing - Review & Editing. **Maria Giorgia Cutrufello:** Conceptualization, Validation, Writing - Review & Editing. **António Maurício Fonseca:** Resources, Writing - Review & Editing. **Angela Martins:** Formal analysis, Validation. **Elisabetta Rombi:** Conceptualization, Supervision, Resources, Writing - Review & Editing.

Conflicts of interest

The authors declare that they have no known competing financial interests or personal relationships that could have appeared to influence the work reported in this paper.

Acknowledgments

This research work has been funded by national funds from FCT/MCTES (PIDDAC) over the projects: Centre of Chemistry (UID/QUI/0686/2020), CEB (UIDB/04469/2020) and project BioTecNorte (operation NORTE-01-0145-FEDER-000004), supported by the Norte Portugal Regional Operational Program (NORTE 2020), under the PORTUGAL 2020 Partnership Agreement, through the European Regional Development Fund (ERDF). The study was also supported by the projects UIDB/00100/2020, (https://doi.org/10.54499/UIDB/00100/2020), UIDP/00100/2020, (https://doi.org/10.54499/UIDP/00100/2020), and LA/P/0056/2020, (https://doi.org/10.54499/LA/P/0056/2020) financed by Fundação para a Ciência e Tecnologia (FCT) to Centro de Química Estrutural.

5. References

[1] R. Ciriminna, C. Della Pina, M. Rossi, M. Pagliaro, Understanding the glycerol market, Eur. J. Lipid Sci. Technol. 116 (2014) 1432–1439 https://doi.org/10.1002/ejlt.201400229

[2] C.H. Zhou, H. Zhao, D.S Tong, L.M Wu, W.H. Yu, Recent Advances in Catalytic Conversion of Glycerol, Catal. Rev.: Sci. and Eng. 55 (2013) 369–453 https://doi.org/10.1080/01614940.2013.816610

[3] G. Dodekatos, S. Schünemann, H. Tüysüz, Recent Advances in Thermo-, Photo-, and Electrocatalytic Glycerol Oxidation, ACS Catal. 8 (2017) 6301–6333 http://dx.doi.org/10.1021/acscatal.8b01317

[4] C. Liu, M. Hiroara, T. Maekawa, R. Chang, T. Hayashi, C. Chiang, Selective electro-oxidation of Glycerol by non-precious electrocatalyst – CuO, Appl. Catal. B: Env. 265 (2020) 118543 https://doi.org/10.1016/j.apcatb.2019.118543

[5] G.W. Crabtree, M.S. Dresselhaus, M.V. Bunchanan, The Hydrogen Economy, Phys. Today, 57 (2004) 39-44 https://doi.org/10.1063/1.1878333

[6] E. Fabbri, K. Habereder, R. Waltar, R. Kötz, T.J. Schmidt, Developments and perspective of oxide-based catalysts for the oxygen evolution reaction, Catal. Sci. Technol. 4 (2014) 3800-3821 https://doi.org/10.1039/C4CY00669K

[7] S. Sun, Y. Zhou, B. Hu, Q. Zhang, Z.J. Xu, Ethylene glycol and ethanol oxidation on spinel Ni-Co oxides in alkaline, J. Electroanal. Chem. 563 (2004) 81-89 https://doi.org/10.1149/2.0761602jes

[8] S. Sun, Z.J. Xu, Composition Dependence of methanol oxidation activity in nickel-cobalt hydroxides and oxides: an optimization toward highly active electrodes, Electrochim. Acta, 165 (2015) 56-66 http://dx.doi.org/10.1016/j.electacta.2015.03.008

[9] J. Deng, Z. Zhou, C. Huang, Factors affecting the catalytic activity of Pd-based electrocatalysts in the electrooxidation of Glycerol: element doping and functional groups on the support, React. Kinet. Mech. Catal. 132 (2021) 1151-1164 http://dx.doi.org/10.1007/s11144-021-01965-2

[10] L. Prati, A. Villa, F. Porta, D. Wang, D. Su, Single-Phase gold/palladium catalysts: The nature of synergistic effect, Catal. Today, 122 (2007) 386-390 http://dx.doi.org/10.1016/j.cattod.2006.11.003

[11] Y. Kwon, K.J.P. Schouten, M.T.M Koper, Mechanism of the catalytic oxidation on polycrystalline gold and platinum electrodes, Chem. Cat. Chem. 3 (2011) 1176-1185 http://dx.doi.org/10.1002/cctc.201100023

[12] M.S.E. Houache, A. Shubair, M.G. Sandoval, R. Safari, G.A. Botton, P.V. Jasen, E.A. González, E.A. Baranova, Influence of Pd and Au on electrochemical valorization of glycerol over Ni-rich surfaces, J. Catal. 396 (2021) 1-13 http://dx.doi.org/10.1016/j.jcat.2021.02.008

[13] A.N. Vyas, G.D. Saratale, S.D Sartale, Recent developments in nickel based electrocatalysts for ethanol electrooxidation, Int. J. Hydrogen Energy, 45 (2020) 5928-5947 https://doi.org/10.1016/j.ijhydene.2019.08.218

[14] M.T. Bender, Y.C. Lam, S. Hammes-Schiffer, K.-S. Choi, Unravelling two pathways for electrochemical alcohol and aldehyde oxidation on NiOOH, J. Am. Chem. Soc. 142 (2020) 21538-21547 https://doi.org/10.1021/jacs.0c10924

[15] V.L. Oliveira, C. Morais, K. Servant, T.W. Napporn, P. Olivi, K.B. Kokoh, G. Tremiliosi-Filho, Kinetic Investigation of Glycerol Oxidation Reaction on Ni/C, Electrocatalysis 6 (2015) 447-454 http://dx.doi.org/10.1007%2Fs12678-015-0261-2

[16] V.L. Oliveira, C. Morais, K. Servant, T.W. Napporn, G. Tremiliosi-Filho, K.B. Kokoh, Studies of the reaction products resulted from glycerol electrooxidation on Ni-based materials in alkaline medium; Electrochim. Acta, 117 (2014) 255-262 http://dx.doi.org/10.1016/j.electacta.2013.11.127

[17] J. Zhang, Y. Shen, Electro-oxidation of glycerol into formic acid by nickel-copper electrocatalysts; J. Electrochem. Soc. 168 (2021) 084510 http://dx.doi.org/10.1149/1945-7111/ac1cfd

[18] M.P. Singh, G.S. Baghel, S.J.J. Titinchi, H.S. Abbo, Zeolites: Smart Materials for Novel, Efficient, and Versatile Catalysis; in Advanced Catalytic Materials, Wyley, 2015, Chapter 11 http://dx.doi.org/10.1002/9781118998939.ch11

[19] A. Araújo, O.S.G.P. Soares, C.A. Orge, A.G Gonçalves, E. Rombi, M.G. Cutrufello, A.M. Fonseca, M.F.R. Pereira, I.C. Neves, Metal-zeolite catalysts for the removal of pharmaceutical pollutants in water by catalytic ozonation, J. Environ. Chem. Eng. 9 (2021) 106458 https://doi.org/10.1016/j.jece.2021.106458

[20] K. Li, J. Valla, J. García-Martínez, Realizing the commercial potential of hierarchical zeolites: New opportunities in catalytic cracking, ChemCatChem, 6 (2014) 46-66 http://dx.doi.org/10.1002/cctc.201300345

[21] M.A. Andrade, L.M.S Ansari, A.J.L. Pombeiro, A.P. Carvalho, A. Martins, L.M.D.R.S. Martins, Fe@Hierarchical BEA Zeolite Catalyst for MW-Assisted Alcohol Oxidation Reaction: A Greener Approach; Catal. 10 (2020) 1029 https://doi.org/10.3390/catal10091029

[22] A. Martins, V. Neves, J. Moutinho, N. Nunes, A.P. Carvalho, Friedel-Crafts acylation reaction over hierarchical Y zeolites modified through surfactant mediated technology, Microporous Mesoporous Mater. 323 (2021) 111167 http://dx.doi.org/10.1016/j.micromeso.2021.111167

[23] A. Martins, B. Amaro, M.S.C.S. Santos, N. Nunes, R. Elvas-Leitão, A.P. Carvalho, Hierarchical Zeolites Prepared Using a Surfactant-Mediated Strategy: ZSM-5 vs. Y as Catalysts for Friedel-Crafts Acylation Reaction, Mol. 29 (2024) 517 http://dx.doi.org/10.3390/molecules29020517

[24] ASTM D3906-03, Standard test method for determination of relative X-Ray diffraction intensities of faujasite-type zeolite-containing materials, 2013 https://doi.org/10.1520/D3906-03R13

[25] ASTM D5758-01, Standard test method for determination of relative crystallinity of zeolite ZSM-5 by X-Ray diffraction. West Conshohocken, 2015. https://doi.org/10.1520/D5758-01R15

[26] J. Gregg, K. Sing, Adsorption, Surface Area and Porosity, Second ed., Academic Press, London, 1982

[27] Z. Mojović, P. Bancović, N. Jović-Jovićić, A. Milutinović-Nikolić, A. Abu Rabi-Stanković, D. Jovanović, Electrocatalytic behavior of nickel impregnated zeolite electrode, Int. J. Hydrogen Energy, 36 (2011) 13343-13351 https://doi.org/10.1016/j.ijhydene.2011.07.097

[28] J. Hessels, F. Yu, R.J. Detz, J.M.H. Reek, Potential- and Buffer-Dependent Catalysts Decomposition during Nickel-Based Water Oxidation Catalysis, Chem. Sus. Chem. 13 (2020) 5625-2631 https://doi.org/10.1002/cssc.202001428

[29] O. Diaz-Morales, D. Ferrus-Suspedra, M.T.M. Koper, The importance of nickel oxyhydroxide deprotonation on its activity towards electrochemical water oxidation, Chem. Sci. 7 (2016) 2639 http://dx.doi.org/10.1039/C5SC04486C

[30] Y. Yan, R. Wang, Q. Zheng, J. Zhong, W. Hao, S. Yan, Z. Zou, Nonredox trivalent nickel catalyzing nucleophilic electrooxidation of organics, Nat. Commun. 14 (2023) 7987. https://doi.org/10.1038/s41467-023-43649-6

[31] A.J. Maia, B. Louis, Y.L. Lam, M.M. Pereira, Ni-ZSM-5 catalysts: Detailed characterization of metal sites for proper catalyst design, J. Catal. 269 (2010) 103-109. https://doi.org/10.1016/j.jcat.2009.10.021